

Disappearance of partonic collectivity in $\sqrt{s_{NN}} = 3 \text{ GeV}$ Au+Au collisions at RHIC

M. S. Abdallah,⁵ B. E. Aboona,⁵⁵ J. Adam,⁶ L. Adamczyk,² J. R. Adams,³⁹ J. K. Adkins,³⁰ G. Agakishiev,²⁸ I. Aggarwal,⁴¹ M. M. Aggarwal,⁴¹ Z. Ahammed,⁶⁰ I. Alekseev,^{3,35} D. M. Anderson,⁵⁵ A. Aparin,²⁸ E. C. Aschenauer,⁶ M. U. Ashraf,¹¹ F. G. Atetalla,²⁹ A. Attri,⁴¹ G. S. Averichev,²⁸ V. Bairathi,⁵³ W. Baker,¹⁰ J. G. Ball Cap,²⁰ K. Barish,¹⁰ A. Behera,⁵² R. Bellwied,²⁰ P. Bhagat,²⁷ A. Bhasin,²⁷ J. Bielcik,¹⁴ J. Bielcikova,³⁸ I. G. Bordyuzhin,³ J. D. Brandenburg,⁶ A. V. Brandin,³⁵ I. Bunzarov,²⁸ J. Butterworth,⁴⁵ X. Z. Cai,⁵⁰ H. Caines,⁶³ M. Calderón de la Barca Sánchez,⁸ D. Cebra,⁸ I. Chakaberia,^{31,6} P. Chaloupka,¹⁴ B. K. Chan,⁹ F-H. Chang,³⁷ Z. Chang,⁶ N. Chankova-Bunzarova,²⁸ A. Chatterjee,¹¹ S. Chattopadhyay,⁶⁰ D. Chen,¹⁰ J. Chen,⁴⁹ J. H. Chen,¹⁸ X. Chen,⁴⁸ Z. Chen,⁴⁹ J. Cheng,⁵⁷ M. Chevalier,¹⁰ S. Choudhury,¹⁸ W. Christie,⁶ X. Chu,⁶ H. J. Crawford,⁷ M. Csanád,¹⁶ M. Daugherty,¹ T. G. Dedovich,²⁸ I. M. Deppner,¹⁹ A. A. Derevschikov,⁴³ A. Dhamija,⁴¹ L. Di Carlo,⁶² L. Didenko,⁶ P. Dixit,²² X. Dong,³¹ J. L. Drachenberg,¹ E. Duckworth,²⁹ J. C. Dunlop,⁶ N. Elsey,⁶² J. Engelage,⁷ G. Eppley,⁴⁵ S. Esumi,⁵⁸ O. Evdokimov,¹² A. Ewigleben,³² O. Eyser,⁶ R. Fatemi,³⁰ F. M. Fawzi,⁵ S. Fazio,⁶ P. Federic,³⁸ J. Fedorisin,²⁸ C. J. Feng,³⁷ Y. Feng,⁴⁴ P. Filip,²⁸ E. Finch,⁵¹ Y. Fisyrak,⁶ A. Francisco,⁶³ C. Fu,¹¹ L. Fulek,² C. A. Gagliardi,⁵⁵ T. Galatyuk,¹⁵ F. Geurts,⁴⁵ N. Ghimire,⁵⁴ A. Gibson,⁵⁹ K. Gopal,²³ X. Gou,⁴⁹ D. Grosnick,⁵⁹ A. Gupta,²⁷ W. Guryn,⁶ A. I. Hamad,²⁹ A. Hamed,⁵ Y. Han,⁴⁵ S. Harabasz,¹⁵ M. D. Harasty,⁸ J. W. Harris,⁶³ H. Harrison,³⁰ S. He,¹¹ W. He,¹⁸ X. H. He,²⁶ Y. He,⁴⁹ S. Heppelmann,⁸ S. Heppelmann,⁴² N. Herrmann,¹⁹ E. Hoffman,²⁰ L. Holub,¹⁴ Y. Hu,¹⁸ H. Huang,³⁷ H. Z. Huang,⁹ S. L. Huang,⁵² T. Huang,³⁷ X. Huang,⁵⁷ Y. Huang,⁵⁷ T. J. Humanic,³⁹ G. Igo,^{9,*} D. Isenhower,¹ W. W. Jacobs,²⁵ C. Jena,²³ A. Jentsch,⁶ Y. Ji,³¹ J. Jia,^{6,52} K. Jiang,⁴⁸ X. Ju,⁴⁸ E. G. Judd,⁷ S. Kabana,⁵³ M. L. Kabir,¹⁰ S. Kagamaster,³² D. Kalinkin,^{25,6} K. Kang,⁵⁷ D. Kapukchyan,¹⁰ K. Kauder,⁶ H. W. Ke,⁶ D. Keane,²⁹ A. Kechechyan,²⁸ M. Kelsey,⁶² Y. V. Khyzhniak,³⁵ D. P. Kikola,⁶¹ C. Kim,¹⁰ B. Kimelman,⁸ D. Kincses,¹⁶ I. Kisel,¹⁷ A. Kiselev,⁶ A. G. Knospe,³² H. S. Ko,³¹ L. Kochenda,³⁵ L. K. Kosarzewski,¹⁴ L. Kramerik,¹⁴ P. Kravtsov,³⁵ L. Kumar,⁴¹ S. Kumar,²⁶ R. Kunnawalkam Elayavalli,⁶³ J. H. Kwasizur,²⁵ R. Lacey,⁵² S. Lan,¹¹ J. M. Landgraf,⁶ J. Lauret,⁶ A. Lebedev,⁶ R. Lednicky,^{28,38} J. H. Lee,⁶ Y. H. Leung,³¹ C. Li,⁴⁹ C. Li,⁴⁸ W. Li,⁴⁵ X. Li,⁴⁸ Y. Li,⁵⁷ X. Liang,¹⁰ Y. Liang,²⁹ R. Licensik,³⁸ T. Lin,⁴⁹ Y. Lin,¹¹ M. A. Lisa,³⁹ F. Liu,¹¹ H. Liu,²⁵ H. Liu,¹¹ P. Liu,⁵² T. Liu,⁶³ X. Liu,³⁹ Y. Liu,⁵⁵ Z. Liu,⁴⁸ T. Ljubicic,⁶ W. J. Llope,⁶² R. S. Longacre,⁶ E. Loyd,¹⁰ N. S. Lukow,⁵⁴ X. F. Luo,¹¹ L. Ma,¹⁸ R. Ma,⁶ Y. G. Ma,¹⁸ N. Magdy,¹² D. Mallick,³⁶ S. Margetis,²⁹ C. Markert,⁵⁶ H. S. Matis,³¹ J. A. Mazer,⁴⁶ N. G. Minaev,⁴³ S. Mioduszewski,⁵⁵ B. Mohanty,³⁶ M. M. Mondal,⁵² I. Mooney,⁶² D. A. Morozov,⁴³ A. Mukherjee,¹⁶ M. Nagy,¹⁶ J. D. Nam,⁵⁴ Md. Nasim,²² K. Nayak,¹¹ D. Neff,⁹ J. M. Nelson,⁷ D. B. Nemes,⁶³ M. Nie,⁴⁹ G. Nigmatkulov,³⁵ T. Niida,⁵⁸ R. Nishitani,⁵⁸ L. V. Nogach,⁴³ T. Nonaka,⁵⁸ A. S. Nunes,⁶ G. Odyniec,³¹ A. Ogawa,⁶ S. Oh,³¹ V. A. Okorokov,³⁵ B. S. Page,⁶ R. Pak,⁶ J. Pan,⁵⁵ A. Pandav,³⁶ A. K. Pandey,⁵⁸ Y. Panebratsev,²⁸ P. Parfenov,³⁵ B. Pawlik,⁴⁰ D. Pawlowska,⁶¹ H. Pei,¹¹ C. Perkins,⁷ L. Pinsky,²⁰ R. L. Pintér,¹⁶ J. Pluta,⁶¹ B. R. Pokhrel,⁵⁴ G. Pomatkin,³⁸ J. Porter,³¹ M. Posik,⁵⁴ V. Prozorova,¹⁴ N. K. Pruthi,⁴¹ M. Przybycien,² J. Putschke,⁶² H. Qiu,²⁶ A. Quintero,⁵⁴ C. Racz,¹⁰ S. K. Radhakrishnan,²⁹ N. Raha,⁶² R. L. Ray,⁵⁶ R. Reed,³² H. G. Ritter,³¹ M. Robotkova,³⁸ O. V. Rogachevskiy,²⁸ J. L. Romero,⁸ D. Roy,⁴⁶ L. Ruan,⁶ J. Rusnak,³⁸ N. R. Sahoo,⁴⁹ H. Sako,⁵⁸ S. Salur,⁴⁶ J. Sandweiss,^{63,*} S. Sato,⁵⁸ W. B. Schmidke,⁶ N. Schmitz,³³ B. R. Schweid,⁵² F. Seck,¹⁵ J. Seger,¹³ M. Sergeeva,⁹ R. Seto,¹⁰ P. Seyboth,³³ N. Shah,²⁴ E. Shahaliev,²⁸ P. V. Shanmuganathan,⁶ M. Shao,⁴⁸ T. Shao,¹⁸ A. I. Sheikh,²⁹ D. Shen,⁵⁰ S. S. Shi,¹¹ Y. Shi,⁴⁹ Q. Y. Shou,¹⁸ E. P. Sichtermann,³¹ R. Sikora,² M. Simko,³⁸ J. Singh,⁴¹ S. Singha,²⁶ M. J. Skoby,⁴⁴ N. Smirnov,⁶³ Y. Söhngen,¹⁹ W. Solyst,²⁵ P. Sorensen,⁶ H. M. Spinka,^{4,*} B. Srivastava,⁴⁴ T. D. S. Stanislaus,⁵⁹ M. Stefaniak,⁶¹ D. J. Stewart,⁶³ M. Strikhanov,³⁵ B. Stringfellow,⁴⁴ A. A. P. Suaide,⁴⁷ M. Sumner,³⁸ B. Summa,⁴² X. M. Sun,¹¹ X. Sun,¹² Y. Sun,⁴⁸ Y. Sun,²¹ B. Surrow,⁵⁴ D. N. Svirida,³ Z. W. Sweger,⁸ P. Szymanski,⁶¹ A. H. Tang,⁶ Z. Tang,⁴⁸ A. Taranenko,³⁵ T. Tarnowsky,³⁴ J. H. Thomas,³¹ A. R. Timmins,²⁰ D. Tlusty,¹³ T. Todoroki,⁵⁸ M. Tokarev,²⁸ C. A. Tomkiel,³² S. Trentalange,⁹ R. E. Tribble,⁵⁵ P. Tribedy,⁶ S. K. Tripathy,¹⁶ T. Truhlar,¹⁴ B. A. Trzeciak,¹⁴ O. D. Tsai,⁹ Z. Tu,⁶ T. Ullrich,⁶ D. G. Underwood,^{4,59} I. Upsal,^{49,6} G. Van Buren,⁶ J. Vanek,³⁸ A. N. Vasiliev,⁴³ I. Vassiliev,¹⁷ V. Verkest,⁶² F. Videbæk,⁶ S. Vokal,²⁸ S. A. Voloshin,⁶² F. Wang,⁴⁴ G. Wang,⁹ J. S. Wang,²¹ P. Wang,⁴⁸ Y. Wang,¹¹ Y. Wang,⁵⁷ Z. Wang,⁴⁹ J. C. Webb,⁶ P. C. Weidenkaff,¹⁹ L. Wen,⁹ G. D. Westfall,³⁴ H. Wieman,³¹ S. W. Wissink,²⁵ J. Wu,²⁶ Y. Wu,¹⁰ B. Xi,⁵⁰ Z. G. Xiao,⁵⁷ G. Xie,³¹ W. Xie,⁴⁴ H. Xu,²¹ N. Xu,³¹ Q. H. Xu,⁴⁹ Y. Xu,⁴⁹ Z. Xu,⁶ Z. Xu,⁹ C. Yang,⁴⁹ Q. Yang,⁴⁹ S. Yang,⁴⁵ Y. Yang,³⁷ Z. Ye,⁴⁵ Z. Ye,¹² L. Yi,⁴⁹ K. Yip,⁶ Y. Yu,⁴⁹ H. Zbroszczyk,⁶¹ W. Zha,⁴⁸ C. Zhang,⁵² D. Zhang,¹¹ J. Zhang,⁴⁹ S. Zhang,¹² S. Zhang,¹⁸ X. P. Zhang,⁵⁷ Y. Zhang,²⁶ Y. Zhang,⁴⁸ Y. Zhang,¹¹ Z. J. Zhang,³⁷ Z. Zhang,⁶ Z. Zhang,¹² J. Zhao,⁴⁴ C. Zhou,¹⁸ X. Zhu,⁵⁷ M. Zurek,⁴ and M. Zyzak¹⁷

(STAR Collaboration)

- ¹Abilene Christian University, Abilene, Texas 79699
- ²AGH University of Science and Technology, FPACS, Cracow 30-059, Poland
- ³Alikhanov Institute for Theoretical and Experimental Physics NRC "Kurchatov Institute", Moscow 117218, Russia
- ⁴Argonne National Laboratory, Argonne, Illinois 60439
- ⁵American University of Cairo, New Cairo 11835, New Cairo, Egypt
- ⁶Brookhaven National Laboratory, Upton, New York 11973
- ⁷University of California, Berkeley, California 94720
- ⁸University of California, Davis, California 95616
- ⁹University of California, Los Angeles, California 90095
- ¹⁰University of California, Riverside, California 92521
- ¹¹Central China Normal University, Wuhan, Hubei 430079
- ¹²University of Illinois at Chicago, Chicago, Illinois 60607
- ¹³Creighton University, Omaha, Nebraska 68178
- ¹⁴Czech Technical University in Prague, FNSPE, Prague 115 19, Czech Republic
- ¹⁵Technische Universität Darmstadt, Darmstadt 64289, Germany
- ¹⁶ELTE Eötvös Loránd University, Budapest, Hungary H-1117
- ¹⁷Frankfurt Institute for Advanced Studies FIAS, Frankfurt 60438, Germany
- ¹⁸Fudan University, Shanghai, 200433
- ¹⁹University of Heidelberg, Heidelberg 69120, Germany
- ²⁰University of Houston, Houston, Texas 77204
- ²¹Huzhou University, Huzhou, Zhejiang 313000
- ²²Indian Institute of Science Education and Research (IISER), Berhampur 760010, India
- ²³Indian Institute of Science Education and Research (IISER) Tirupati, Tirupati 517507, India
- ²⁴Indian Institute Technology, Patna, Bihar 801106, India
- ²⁵Indiana University, Bloomington, Indiana 47408
- ²⁶Institute of Modern Physics, Chinese Academy of Sciences, Lanzhou, Gansu 730000
- ²⁷University of Jammu, Jammu 180001, India
- ²⁸Joint Institute for Nuclear Research, Dubna 141 980, Russia
- ²⁹Kent State University, Kent, Ohio 44242
- ³⁰University of Kentucky, Lexington, Kentucky 40506-0055
- ³¹Lawrence Berkeley National Laboratory, Berkeley, California 94720
- ³²Lehigh University, Bethlehem, Pennsylvania 18015
- ³³Max-Planck-Institut für Physik, Munich 80805, Germany
- ³⁴Michigan State University, East Lansing, Michigan 48824
- ³⁵National Research Nuclear University MEPhI, Moscow 115409, Russia
- ³⁶National Institute of Science Education and Research, HBNI, Jatni 752050, India
- ³⁷National Cheng Kung University, Tainan 70101
- ³⁸Nuclear Physics Institute of the CAS, Rez 250 68, Czech Republic
- ³⁹Ohio State University, Columbus, Ohio 43210
- ⁴⁰Institute of Nuclear Physics PAN, Cracow 31-342, Poland
- ⁴¹Panjab University, Chandigarh 160014, India
- ⁴²Pennsylvania State University, University Park, Pennsylvania 16802
- ⁴³NRC "Kurchatov Institute", Institute of High Energy Physics, Protvino 142281, Russia
- ⁴⁴Purdue University, West Lafayette, Indiana 47907
- ⁴⁵Rice University, Houston, Texas 77251
- ⁴⁶Rutgers University, Piscataway, New Jersey 08854
- ⁴⁷Universidade de São Paulo, São Paulo, Brazil 05314-970
- ⁴⁸University of Science and Technology of China, Hefei, Anhui 230026
- ⁴⁹Shandong University, Qingdao, Shandong 266237
- ⁵⁰Shanghai Institute of Applied Physics, Chinese Academy of Sciences, Shanghai 201800
- ⁵¹Southern Connecticut State University, New Haven, Connecticut 06515
- ⁵²State University of New York, Stony Brook, New York 11794
- ⁵³Instituto de Alta Investigación, Universidad de Tarapacá, Arica 1000000, Chile
- ⁵⁴Temple University, Philadelphia, Pennsylvania 19122
- ⁵⁵Texas A&M University, College Station, Texas 77843
- ⁵⁶University of Texas, Austin, Texas 78712
- ⁵⁷Tsinghua University, Beijing 100084
- ⁵⁸University of Tsukuba, Tsukuba, Ibaraki 305-8571, Japan
- ⁵⁹Valparaiso University, Valparaiso, Indiana 46383
- ⁶⁰Variable Energy Cyclotron Centre, Kolkata 700064, India
- ⁶¹Warsaw University of Technology, Warsaw 00-661, Poland
- ⁶²Wayne State University, Detroit, Michigan 48201

⁶³Yale University, New Haven, Connecticut 06520

We report on the measurements of directed flow v_1 and elliptic flow v_2 for hadrons (π^\pm , K^\pm , K_S^0 , p , ϕ , Λ and Ξ^-) from Au+Au collisions at $\sqrt{s_{NN}} = 3$ GeV and v_2 for (π^\pm , K^\pm , p and \bar{p}) at 27 and 54.4 GeV with the STAR experiment. While at the two higher energy midcentral collisions the number-of-constituent-quark (NCQ) scaling holds, at 3 GeV the midrapidity v_2 is negative for all hadrons and the NCQ scaling is absent. In addition, the midrapidity v_1 slopes for almost all observed hadrons are found to be positive, implying dominant repulsive baryonic interactions. The features of negative v_2 and positive v_1 slope at 3 GeV can be reproduced with a baryonic mean-field in transport model calculations. These results imply that in 3 GeV Au+Au collisions, the medium is characterized by baryonic interactions.

Relativistic heavy-ion collisions at the Large Hadron Collider (LHC) and the Relativistic Heavy Ion Collider (RHIC), where the net-baryon density is low, are generally considered to have produced a new form of matter with partonic degrees of freedom, usually referred to as the Quark Gluon Plasma (QGP) [1–5]. However, it is necessary to identify changes in matter properties, *e.g.* in its equation of state (EOS), before ultimately claiming the discovery of the QGP. Locating the onset of the QGP, exploring the nature of the phase transition from hadronic matter to the QGP, and understanding the Quantum Chromodynamics (QCD) phase diagram at finite net-baryon densities, is an area of active experimental research and the focus of the RHIC Beam Energy Scan Phase II (BES-II) [6]. This is, after the discovery of the QGP at vanishing net-baryon density, an important step toward understanding the phase structure of nuclear matter in the high baryon density region.

Anisotropic flows (v_n) [7–9], the first two components of which are called directed flow (v_1) and elliptic flow (v_2), are among the most effective tools to study the properties of the QCD matter created in heavy-ion collisions. They are generated early in the system evolution, and are sensitive probes of the EOS of the produced medium [10–12]. At higher energies (nucleon-nucleon center-of-mass energy $\sqrt{s_{NN}} \gtrsim 27$ GeV), where the transit time of the colliding nuclei ($\sim 2R/\gamma\beta$) is smaller than the typical production time of particles [13, 14], flow harmonics are dominated by the collective expansion of initial partonic density distribution [15–17]. At lower energies, shadowing effect by the passing spectator nucleons becomes important [18–23]. At $\sqrt{s_{NN}} \lesssim 4$ GeV, nuclear mean-field effects will contribute to the observed azimuthal anisotropies [24–27]. Previous studies have shown that v_1 and v_2 are particularly sensitive to nuclear incompressibility (κ) in the high baryon density region [28–30]. The constraints on κ by comparing experimental data with results from the theoretical transport model will certainly help us to understand nuclear EOS.

Large positive v_2 along with the observation of its number-of-constituent-quarks (NCQ) scaling are strong evidence for the formation of a hydrodynamically expanding QGP phase with partonic degrees of freedom [15–17]. Positive v_2 of light hadrons at midrapidity has been observed from the top RHIC energy

down to 4.5 GeV [23]. On the other hand, at $\sqrt{s_{NN}} \geq 10$ GeV, all midrapidity v_1 slopes are found to have negative values and approach to zero with increasing energy [20, 21, 31], where partonic collectivity is dominant. At lower collision energies the v_1 slope values for baryons become positive, while those for mesons remain negative [18, 23, 32, 33]. For example, results of proton and light nuclei v_1 and v_2 from $\sqrt{s_{NN}} = 2.4$ GeV Au+Au collisions were reported recently by the HADES experiment [34].

In this letter we report systematic results of v_1 and v_2 for identified hadrons (π^\pm , K^\pm , K_S^0 , p , ϕ , Λ , and Ξ^-) from 10-40% centrality Au+Au collisions at $\sqrt{s_{NN}} = 3$ GeV and v_2 of (π^\pm , K^\pm , p , and \bar{p}) at $\sqrt{s_{NN}} = 27$ and 54.4 GeV from the STAR experiment. The data sets at 3, 27, and 54.4 GeV are 260, 560, and 600 $\times 10^6$ events with minimum-bias trigger, respectively. The main detector of STAR is a cylindrical Time Projection Chamber (TPC) [35] 4 m in diameter and 4 m in length. The TPC resides in a solenoidal magnet providing a uniform magnetic field of 0.5 T along the longitudinal beam direction. The 3 GeV data were taken, with beam energy of 3.85 GeV per nucleon, in 2018 in the fixed-target (FXT) mode. The target is positioned inside the beam pipe near the edge of the TPC, at 200 cm from the TPC center along the beam axis. This gives an experimental acceptance coverage of $0 < \eta < 2$ in pseudorapidity. The higher energy data were taken in the collider mode, where the beam bunch crossing was restricted to the TPC central region, yielding an acceptance of $|\eta| < 1$.

The centrality of collisions is characterized by the number of charged tracks detected with the TPC within pseudorapidity $|\eta| < 0.5$ in collider mode collisions and $0 < \eta < 2$ for FXT mode collisions. In order to remove the pile-up effect, events with multiplicity greater than 195 are excluded from the analysis at $\sqrt{s_{NN}} = 3$ GeV. The primary vertex position of each event along the beam direction, V_z , is required to be within ± 40 cm of the center of the TPC at $\sqrt{s_{NN}} = 27$ and 54.4 GeV, and within ± 2 cm of the target position for the FXT mode collisions at $\sqrt{s_{NN}} = 3$ GeV. An additional selection on the primary vertex position within a radius less than 2 cm is required to eliminate possible beam interactions with the vacuum pipe [4-cm radius] at all three energies. In order to improve the track quality, momentum and ionization energy

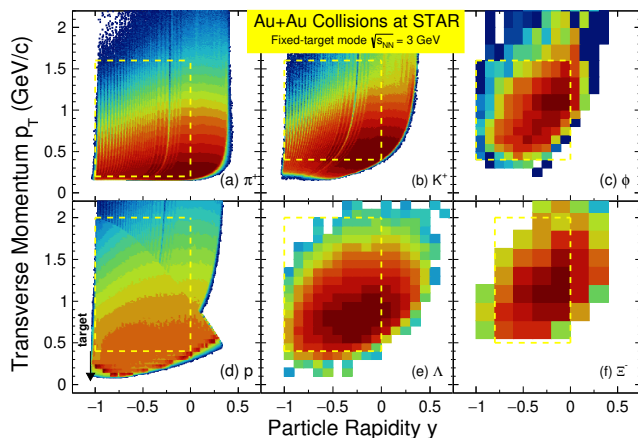


FIG. 1. The acceptance in transverse momentum (p_T) and identified particle rapidity (y) for π^+ , K^+ , ϕ , p , Λ and Ξ^- measured with the STAR detector TPC and TOF in Au+Au collisions at $\sqrt{s_{NN}} = 3$ GeV, with the FXT mode of beam energy 3.85 GeV per nucleon. The target is located at $y = -1.05$. In each plot, intensity is self-normalized.

loss resolution from the TPC, the following track selections are applied: i) the number of hit points is larger than 15; ii) the ratio between the number of hit points and the maximum possible number of hit points is larger than 0.52; iii) the distance of closest approach (DCA) to the primary vertex is less than 3 cm [22].

The particle identification of charged pions with transverse momentum range $0.2 < p_T < 1.6$ GeV/ c , charged kaons with $0.4 < p_T < 1.6$ GeV/ c , and protons with $0.4 < p_T < 2.0$ GeV/ c are based on ionization energy loss information measured with the TPC detector and time-of-flight information measured with the Time-of-Flight (TOF) detector [36]. Reconstruction of K_S^0 , Λ , and Ξ^- is performed using the KF Particle Finder package based on the Kalman Filter method initially developed for the CBM and ALICE experiments [37], which utilizes the quality of the track fit and the decay topology. The ϕ mesons are reconstructed through the decay channel, $\phi \rightarrow K^+ + K^-$, where the combinatorial background is estimated using the mixed-event technique [22].

Figure 1 presents the acceptance in y and p_T for π^+ , K^+ , p , ϕ , Λ , and Ξ^- , measured with the TPC and TOF detectors in Au+Au collisions at $\sqrt{s_{NN}} = 3$ GeV. The target is located at $y = -1.05$ and the positive sign of v_1 is defined by the forward positive rapidity region. The acceptance for all particles covers from midrapidity to target rapidity. The coverage of p_T is from 0.2 to ~ 2 GeV/ c , depending on the rest mass of the particle.

The second order event plane is reconstructed from tracks recorded by the TPC at $\sqrt{s_{NN}} = 27$ and 54.4 GeV. In order to avoid self-correlation and suppress non-flow effects, the η -subevent plane method [38] is used for the elliptic flow calculation, in which the η ranges $-1 < \eta <$

-0.05 and $0.05 < \eta < 1$ are applied for the two independent subevents, separately. At $\sqrt{s_{NN}} = 3$ GeV, the first order event plane is determined with the Event Plane Detector (EPD) [39] located on the east side of the STAR detector system. The v_1 and v_2 at 3 GeV are determined with the first order event plane. The detailed event plane resolution is shown in the Supplemental Material. The final results are corrected for centrality bin width, event plane resolution, and detector acceptance.

Systematic uncertainties are estimated point-by-point by varying track selection criteria, and the decay length of parent and daughter when using the KF Particle Finder package [37]. At $\sqrt{s_{NN}} = 3$ GeV, the leading systematic source is from particle misidentification by varying the ionization energy loss dE/dx , estimated to contribute 4.3% (1.5%) to π^+ (proton) v_1 slopes measurements. An additional, common systematic uncertainty from event plane resolution is estimated to be 1.4% and 3% for v_1 and v_2 , respectively. Assuming the sources are uncorrelated, the total systematic uncertainty is obtained by adding uncertainties mentioned above in quadrature.

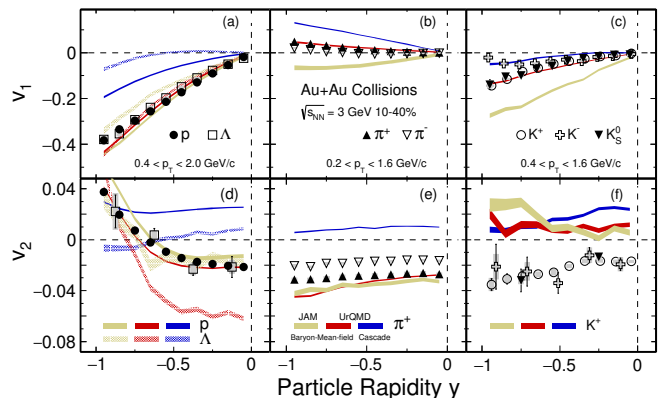


FIG. 2. Rapidity(y) dependence of v_1 (top panels) and v_2 (bottom panels) of proton and Λ baryons (left panels), pions (middle panels) and kaons (right panels) in 10-40% centrality for the $\sqrt{s_{NN}} = 3$ GeV Au+Au collisions. Statistical and systematic uncertainties are shown as bars and gray bands, respectively. Some uncertainties are smaller than the data points. The UrQMD and JAM results are shown as bands: golden, red and blue bands stand for JAM mean-field, UrQMD mean-field and UrQMD cascade mode, respectively. The value of the incompressibility $\kappa = 380$ MeV is used in the mean-field option. More detailed model descriptions and data comparisons can be found in Supplemental Material.

The rapidity dependence of the directed flow v_1 and elliptic flow v_2 of identified hadrons from the $\sqrt{s_{NN}} = 3$ GeV Au+Au collisions at 10-40% is presented in Fig. 2. Due to the acceptance, the results from the rapidity region $-1 < y < 0$ are shown. The corresponding p_T range for each hadron is shown in the figure. For comparison, calculations of transport theoretical model, JET AA Microscopic Transportation Model

(JAM) [40] and Ultra-relativistic Quantum Molecular Dynamics (UrQMD) [25, 26], are also given for the abundantly produced hadrons π^+ , K^+ , p , and Λ . The results from the cascade and baryonic mean-field modes of the JAM and UrQMD model are shown as colored bands. The same collision centrality and kinematic selection criteria as in the data are applied in the model calculations.

From the top panels in Fig. 2 the strength of the rapidity dependence of v_1 is shown to be proportional to the hadron mass. The values of the midrapidity slope, defined as $dv_1/dy|_{y=0}$, are the largest for protons and Λ s, see panel (a), and are close to zero for pions in panel (b). In panel (c), $dv_1/dy|_{y=0}$ are positive and have small charge dependence among kaons. The JAM and UrQMD mean-field calculation includes a Skyrme potential energy density function [30]. Comparing to the cascade mode, the repulsive interactions among baryons are enhanced via an additional mean-field option, resulting in a good agreement with experimental data. A similar conclusion can be drawn for the elliptic flow v_2 . As shown in the lower panels of Fig. 2, all of the measured midrapidity hadrons, ($|y| \leq 0.5$) show negative values of v_2 implying an out-of-plane expansion in the 3 GeV collisions, contrary to the in-plane expansion in high energy collisions [16, 17]. Again, with the mean-field option with $\kappa = 380$ MeV, the JAM and UrQMD model calculations qualitatively reproduce the rapidity dependence of v_2 for baryons and pions. Nevertheless, we note that the UrQMD model overpredicts the strength of v_2 for strange baryon Λ and both JAM and UrQMD model fails to reproduce kaon v_2 , see Fig. 2.

Similar to the previous v_1 studies [20, 21, 41] from the STAR experiment, a polynomial fit of the form $v_1(y) = a + by + cy^3$ was used to extract the strength of directed flow at midrapidity for π^\pm , K^\pm , K_S^0 , p , and Λ , while the fit form $v_1(y) = by$ was used for ϕ and Ξ^- due to the limited statistics. The fit range for all particles is $-0.75 < y < 0$. Hereafter, we refer to $dv_1/dy|_{y=0}$ as the slope obtained from the above fit. The cubic fit term, c , can reduce the sensitivity to the rapidity range. The constant term, a , accounts for the effects from event plane fluctuation and momentum conservation [42]. The constant term, a , is found to be < 0.005 for all particles except ϕ and Ξ^- in the 10-40% centrality.

The elliptic flow scaled by the number of constituent quarks, v_2/n_q , for the copiously produced hadrons π^\pm (squares), K^\pm (crosses), p and \bar{p} (circles) is shown as a function of the scaled transverse kinetic energy $(m_T - m_0)/n_q$ in Fig. 3. Data are from 10-40% mid-central Au+Au collisions at RHIC. Data points from 27 and 54.4 GeV are shown as open and closed symbols, respectively. The colored dashed lines, also displayed in the figure, represent the scaling fit to data for pions, kaons, and protons in 7.7, 14.5, 27, 54.4, and 200 GeV Au+Au collisions [22, 46] for both positive and negative charged particles. Although the overall quark number

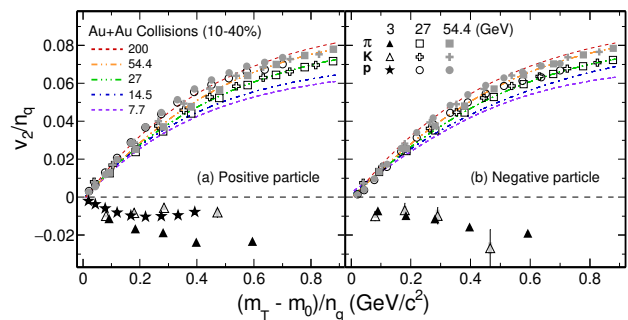


FIG. 3. v_2 scaled by the number of constituent quarks, v_2/n_q , as a function of scaled transverse kinetic energy $((m_T - m_0)/n_q)$ for pions, kaons and protons from Au+Au collisions in 10-40% centrality at $\sqrt{s_{NN}} = 3, 27$, and 54.4 GeV for positive charged particles (left panel) and negative charged particles (right panel). Colored dashed lines represent the scaling fit to data in 7.7, 14.5, 27, 54.4, and 200 GeV Au+Au collisions from STAR experiment at RHIC [43–45]. Statistical and systematic uncertainties are shown as bars and gray bands, respectively. Some uncertainties are smaller than the data points.

scaling is evident, it has been observed that the best scaling is reached in the RHIC top energy $\sqrt{s_{NN}} = 200$ GeV collisions [16]. As the collision energy decreases, the scaling deteriorates. Particles and antiparticles are no longer consistent with the single-particle NCQ scaling [22] due to the mixture of the transported and produced quarks. More detailed discussions on the effects of transported quarks on collectivity can be found in Refs. [20, 47]. As one of the important evidence for the QGP formation in high energy collisions at RHIC, the observed NCQ scaling originates from partonic collectivity [16, 17, 48].

For 3 GeV collisions, data points for π , K and p are represented by filled triangles, open triangles and filled stars, respectively in Fig. 3. It is apparent that all of the values of v_2/n_q are negative. Only proton results are shown, because of the lack of antiproton production at this energy. Contrary to the higher energy data shown, the quark scaling disappears in the observed elliptic flow for positively charged particles in such low energy collisions. The new results clearly indicate different properties for the matter produced. As shown in Fig. 2, the JAM and UrQMD model calculations with baryonic mean-field potential reproduce the observed negative values of v_2 for protons as well as Λ s. In other words, in the 3 GeV collisions, partonic interactions no longer dominate and baryonic scatterings take over. This observation is clear evidence that predominantly hadronic matter is created in such collisions.

The collision energy dependence of the directed and elliptic flow is summarized in Fig. 4. Figure 4(a) shows the p_T -integrated midrapidity directed flow slope $dv_1/dy|_{y=0}$ for π , K , p , Λ and multi-strange hadrons ϕ and Ξ^-

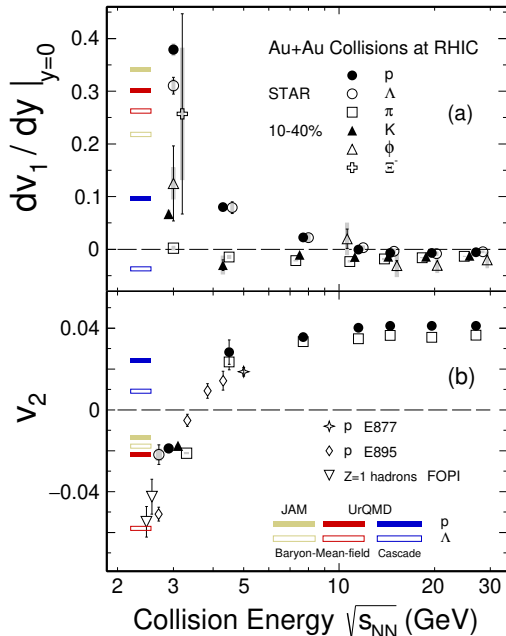


FIG. 4. Collision energy dependence of (top panel) directed flow slope $dv_1/dy|_{y=0}$ for p , Λ , π (combined from π^\pm), K (combined from K^\pm and K_S^0), ϕ and Ξ^- , and (bottom panel) elliptic flow v_2 for p , π (combined from π^\pm) in heavy-ion collisions. Collision centrality for all data from RHIC is 10-40%, except for 4.5 GeV where 10-30% is for $dv_1/dy|_{y=0}$ and 0-30% is for v_2 . Statistical and systematic uncertainties are shown as bars and gray bands, respectively. Some uncertainties are smaller than the data points. The JAM and UrQMD results are shown as colored bands: golden, red and blue bands stand for JAM mean-field, UrQMD mean-field and UrQMD cascade mode, respectively. For clarity the x-axis value of the data points have been shifted.

from Au+Au collisions for the 10-40% centrality interval. Here the positive and negative particle results are combined for both pions and kaons, as the differences between them are small, as shown in Fig. 2. The p_T -integrated midrapidity v_2 of π , K , p and Λ are shown in Fig. 4(b) as open squares, filled triangles, filled circles and open circles, respectively. Due to partonic collectivity in Au+Au collisions at high energy [49], all observed midrapidity v_1 slopes and v_2 are found to be negative and positive, respectively, while the observed trend in Fig. 4 for 3 GeV collisions is exactly the opposite. Results from calculations using the hadronic transport model JAM and UrQMD, with the same centrality and kinematic cuts as used in the data analysis, are also shown as colored bands in the figure. By including the baryonic mean-field, the JAM and UrQMD model reproduced the trends for both $dv_1/dy|_{y=0}$ and v_2 for baryons including protons and Λ . The consistency of transport models (JAM and UrQMD) with baryonic mean-field for all measured baryons implies that the dominant degrees of freedom at 3 GeV are the interacting baryons. The signatures for the transition from

partonic dominant to hadronic and to baryonic dominant regions have also been discussed in Ref. [20, 21, 50, 51] for the ratios of K^+/π^+ and net-particle v_1 slopes, respectively. Our new data clearly reveals that baryonic interactions dictate the collision dynamics in 3 GeV collisions.

In summary, we have reported on the p_T and rapidity differential and integral measurements for directed flow v_1 and elliptic flow v_2 of identified hadrons π^\pm , K^\pm , K_S^0 , ϕ , p , Λ and Ξ^- from the 10-40% centrality Au+Au collisions at $\sqrt{s_{NN}} = 3$ GeV, and the high statistics measurements for v_2 of π^\pm , K^\pm , p and \bar{p} at $\sqrt{s_{NN}} = 27$ and 54.4 GeV. The number of constituent quark (NCQ) scaling of v_2 is observed for collision energies ≥ 7.7 GeV. Due to the formation of the QGP at center-of-mass collision energies larger than 10 GeV, one finds that each hadron's v_2 is positive while all slopes of v_1 are negative. For the 3 GeV collisions, the NCQ scaling is absent and the opposite collective behavior is observed: the midrapidity elliptic flow of all hadrons is negative; the midrapidity slope of the directed flow of all hadrons is positive. Furthermore, transport models JAM and UrQMD calculations with a baryonic mean-field qualitatively reproduced these results. These observations imply the vanishing of partonic collectivity and a new EOS, dominated by baryonic interactions in the high baryon density region.

We thank Drs. Y. Nara and J. Steinheimer for interesting discussions and the use of their JAM and UrQMD simulations codes. We thank the RHIC Operations Group and RCF at BNL, the NERSC Center at LBNL, and the Open Science Grid consortium for providing resources and support. This work was supported in part by the Office of Nuclear Physics within the U.S. DOE Office of Science, the U.S. National Science Foundation, the Ministry of Education and Science of the Russian Federation, National Natural Science Foundation of China, Chinese Academy of Science, the Ministry of Science and Technology of China and the Chinese Ministry of Education, the Higher Education Sprout Project by Ministry of Education at NCKU, the National Research Foundation of Korea, Czech Science Foundation and Ministry of Education, Youth and Sports of the Czech Republic, Hungarian National Research, Development and Innovation Office, New National Excellency Programme of the Hungarian Ministry of Human Capacities, Department of Atomic Energy and Department of Science and Technology of the Government of India, the National Science Centre of Poland, the Ministry of Science, Education and Sports of the Republic of Croatia, RosAtom of Russia and German Bundesministerium für Bildung, Wissenschaft, Forschung und Technologie (BMBF), Helmholtz Association, Ministry of Education, Culture, Sports, Science, and Technology (MEXT) and Japan Society for the Promotion of Science (JSPS).

* Deceased

- [1] I. Arsene *et al.* (BRAHMS), Nucl. Phys. A **757**, 1 (2005).
- [2] K. Adcox *et al.* (PHENIX), Nucl. Phys. A **757**, 184 (2005).
- [3] B. B. Back *et al.* (PHOBOS), Nucl. Phys. A **757**, 28 (2005).
- [4] J. Adams *et al.* (STAR), Nucl. Phys. A **757**, 102 (2005).
- [5] K. Aamodt *et al.* (ALICE), Phys. Rev. Lett. **105**, 252302 (2010).
- [6] STAR Note 0598: BES-II whitepaper. <https://drupal.star.bnl.gov/STAR/starnotes/public/sn0598>.
- [7] H. Sorge, Phys. Rev. Lett. **78**, 2309 (1997).
- [8] H. Sorge, Phys. Lett. B **402**, 251 (1997).
- [9] J.-Y. Ollitrault, Phys. Rev. D **46**, 229 (1992).
- [10] C. M. Hung and E. V. Shuryak, Phys. Rev. Lett. **75**, 4003 (1995).
- [11] J. Steinheimer, J. Auvinen, H. Petersen, M. Bleicher, and H. Stöcker, Phys. Rev. C **89**, 054913 (2014).
- [12] Y. Nara, H. Niemi, A. Ohnishi, and H. Stöcker, Phys. Rev. C **94**, 034906 (2016).
- [13] A. Bialas and M. Gyulassy, Nucl. Phys. B **291**, 793 (1987).
- [14] Z.-W. Lin, Phys. Rev. C **98**, 034908 (2018).
- [15] B. I. Abelev *et al.* (STAR), Phys. Rev. Lett. **99**, 112301 (2007).
- [16] L. Adamczyk *et al.* (STAR), Phys. Rev. Lett. **116**, 062301 (2016).
- [17] L. Adamczyk *et al.* (STAR), Phys. Rev. Lett. **118**, 212301 (2017).
- [18] H. Liu *et al.* (E895), Phys. Rev. Lett. **84**, 5488 (2000).
- [19] C. Pinkenburg *et al.* (E895), Phys. Rev. Lett. **83**, 1295 (1999).
- [20] L. Adamczyk *et al.* (STAR), Phys. Rev. Lett. **120**, 062301 (2018).
- [21] L. Adamczyk *et al.* (STAR), Phys. Rev. Lett. **112**, 162301 (2014).
- [22] L. Adamczyk *et al.* (STAR), Phys. Rev. C **88**, 014902 (2013).
- [23] M. S. Abdallah *et al.* (STAR), Phys. Rev. C **103**, 034908 (2021).
- [24] O. Buss, T. Gaitanos, K. Gallmeister, H. van Hees, M. Kaskulov, O. Lalakulich, A. B. Larionov, T. Leitner, J. Weil, and U. Mosel, Phys. Rept. **512**, 1 (2012).
- [25] S. A. Bass *et al.*, Prog. Part. Nucl. Phys. **41**, 255 (1998).
- [26] M. Bleicher *et al.*, J. Phys. G **25**, 1859 (1999).
- [27] A. Andronic *et al.* (FOPI), Phys. Lett. B **612**, 173 (2005).
- [28] P. Danielewicz, R. Lacey, and W. G. Lynch, Science **298**, 1592 (2002).
- [29] P. Danielewicz, R. A. Lacey, P. B. Gossiaux, C. Pinkenburg, P. Chung, J. M. Alexander, and R. L. McGrath, Phys. Rev. Lett. **81**, 2438 (1998).
- [30] H. Kruse, B. V. Jacak, and H. Stoecker, Phys. Rev. Lett. **54**, 289 (1985).
- [31] J. Brachmann, S. Soff, A. Dumitru, H. Stoecker, J. A. Maruhn, W. Greiner, L. V. Bravina, and D. H. Rischke, Phys. Rev. C **61**, 024909 (2000).
- [32] J. C. Kintner *et al.*, Phys. Rev. Lett. **78**, 4165 (1997).
- [33] P. Chung *et al.* (E895), Phys. Rev. Lett. **85**, 940 (2000).
- [34] J. Adamczewski-Musch *et al.* (HADES), Phys. Rev. Lett. **125**, 262301 (2020).
- [35] M. Anderson *et al.*, Nucl. Instrum. Meth. A **499**, 659 (2003).
- [36] F. Geurts *et al.*, Nucl. Instrum. Meth. A **533**, 60 (2004).
- [37] I. Kisel (CBM), J. Phys. Conf. Ser. **1070**, 012015 (2018).
- [38] A. M. Poskanzer and S. A. Voloshin, Phys. Rev. C **58**, 1671 (1998).
- [39] J. Adams *et al.*, Nucl. Instrum. Meth. A **968**, 163970 (2020).
- [40] Y. Nara, N. Otuka, A. Ohnishi, K. Niita, and S. Chiba, Phys. Rev. C **61**, 024901 (1999).
- [41] L. Adamczyk *et al.* (STAR), Phys. Rev. Lett. **108**, 202301 (2012).
- [42] N. Borghini, P. M. Dinh, J.-Y. Ollitrault, A. M. Poskanzer, and S. A. Voloshin, Phys. Rev. C **66**, 014901 (2002).
- [43] L. Adamczyk *et al.* (STAR), Phys. Rev. Lett. **110**, 142301 (2013).
- [44] L. Adamczyk *et al.* (STAR), Phys. Rev. C **93**, 014907 (2016).
- [45] B. I. Abelev *et al.* (STAR), Phys. Rev. C **77**, 054901 (2008).
- [46] X. Dong, S. Esumi, P. Sorensen, N. Xu, and Z. Xu, Phys. Lett. B **597**, 328 (2004).
- [47] J. C. Dunlop, M. A. Lisa, and P. Sorensen, Phys. Rev. C **84**, 044914 (2011).
- [48] D. Molnar and S. A. Voloshin, Phys. Rev. Lett. **91**, 092301 (2003).
- [49] R. J. M. Snellings, H. Sorge, S. A. Voloshin, F. Q. Wang, and N. Xu, Phys. Rev. Lett. **84**, 2803 (2000).
- [50] A. Bzdak, S. Esumi, V. Koch, J. Liao, M. Stephanov, and N. Xu, Phys. Rep. **853**, 1 (2020).
- [51] L. Adamczyk *et al.* (STAR), Phys. Rev. C **96**, 044904 (2017).